Distribution of active tectonics in the Himalayan piedmont (Darjeeling, Eastern India) inferred from Horizontal-to-Vertical Spectral Ratio analysis of passive seismic records

E. Large, Pascale Huyghe, Jean-louis Mugnier, B. Guillier, S. Taral, B.R. Gyawali, T. Chabraborty

Distribution of active tectonics in the Himalayan piedmont (Darjeeling, Eastern India) inferred from Horizontal-to-Vertical Spectral Ratio analysis of passive seismic records

E. Large[1], P. Huyghe[1], J-L. Mugnier[1], B. Guillier[1], S. Taral[2], B.R. Gyawali[3] and T. Chabraborty[4]

[1]*Institut des Sciences de la Terre, Université Grenoble Alpes/ Université Savoie Mont-Blanc/CNRS/IRD, CS40700, 38058 Grenoble Cedex 9, France*

[2]*Geology & Geophysics Department, Indian Institute of Technology, Kharagpur, India*

[3] *Tri-Chandra Multiple Campus, Tribhuvan University, Nepal*

[4]*Geological Studies Unit, Indian Statistical Institute, Kolkata 700108, India*

Correspondence: *Dr. Pascale Huyghe, Institut des Sciences de la Terre, Université Grenoble Alpes, 1381 rue de la Piscine, 30400 Saint- Martin d'Hères, France.*

E-mail: Pascale.huyghe@univ-grenoble-alpes.fr

Short title: Active tectonics in the Darjeeling piedmont

Statement of significance:

Active tectonics necessitate to select key zones for detailed studies. In the Himalaya, and specially in its piedmont, the quality of natural outcrops is poor due to strong weathering, heavy vegetation and/or anthropogenic influence. In this paper, we show that the HVSR (Horizontal-to-Vertical Spectral Ratio) method allows exploring the structures beneath the

plain south of the Himalayan mountain front. This method is easy to apply in any context and we show that it has allowed revealing the subsurface structures down to 600 meters even in jungle areas. We have correlated geomorphologic scarps evidenced by geomorphologic profiles but nearly invisible in the jungle, to thrust structures evidenced at depth. Two of these scarps of about ten meters affect the 3.7 ± 0.7 ka old surface and imply that about half of the convergence is expressed south of the Himalayan front in this zone.

Key words: Himalayan mountain front, active tectonics, geomorphology, passive seismic records, Horizontal-to-Vertical Spectral Ratio

Abstract

The pattern of active deformation of frontal structures in Darjeeling Himalaya is complex with out-of-sequence reactivations in the chain and development of scarps associated to earthquake ruptures reaching the surface in the piedmont. To clarify the distribution of active deformation in this area, we analyze passive seismic records by the Horizontal-to-Vertical Spectral Ratio method along three NS trending profiles. We image the Siwalik sedimentary rocks / recent deposits interface under the piedmont and show folded and faulted geometries. Two of these faults are located under scarps of about ten meters affecting the 3.7 ± 0.7 ka old surface of the Tista megafan. Such features imply that about half of the convergence is expressed south of the Himalayan front while the other part occurs out-of-sequence in the chain, suggesting a very limited activity of the Main Frontal Thrust itself.

1. Introduction

Studying active tectonics in the Himalayas is of primary importance to assess the seismic hazard related to Himalayan earthquakes that overpass Mw 8 (Bilham, 2019). Indeed, Himalayan tectonics follow a rather simple seismic cycle and display a succession of ruptures along the Main Himalayan Thrust (MHT) that transfer most of the Himalayan convergence to the mountain front during great earthquakes (Bilham, 2019). Therefore, the ~20 mm/yr Holocene shortening is frequently considered as almost entirely concentrated at the front of the Himalayan range (e.g., Lavé and Avouac, 2000) and trenches are performed through the Main Frontal Thrust (MFT), the southern emergent tip of the MHT. While trenching is an effective method for reconstructing the calendar of paleo-earthquakes (e.g., Bollinger et al., 2014) and constraining paleoseismic features, it is often difficult to localize the emergence of

ruptures and the use of preliminary geophysical acquisition methods is necessary to establish the location of paleoseismic trenches. Subsurface structures of the plain south of the Himalayan front have already been imaged by seismic reflection in the first kilometres of sediments (e.g., Duvall et al., 2020; Almeida et al., 2018; Bashyal, 1998) and GPR (Ground Penetrating Radar) documenting 10-20 m depth around fault scarps (Pati et al., 2012).

The objective of this paper is to show the possibility of imaging subsurface structures down to depths of a few hundred meters, using the geophysical Horizontal-to-Vertical Spectral Ratio (HVSR) method (Bard, 1999; Nakamura, 1989). We apply this method in the piedmont of Darjeeling Himalaya (India) where the pattern of active deformation is especially complex (Figure 1). In this area, out-of-sequence reactivations occur in the chain (Mukul, 2000) while recent deformation in the piedmont is distributed over several faults (e.g., Nakata, 1989). Our study from HVSR analysis of passive seismic records therefore localizes subsurface structures allowing a better understanding of the active deformation distribution.

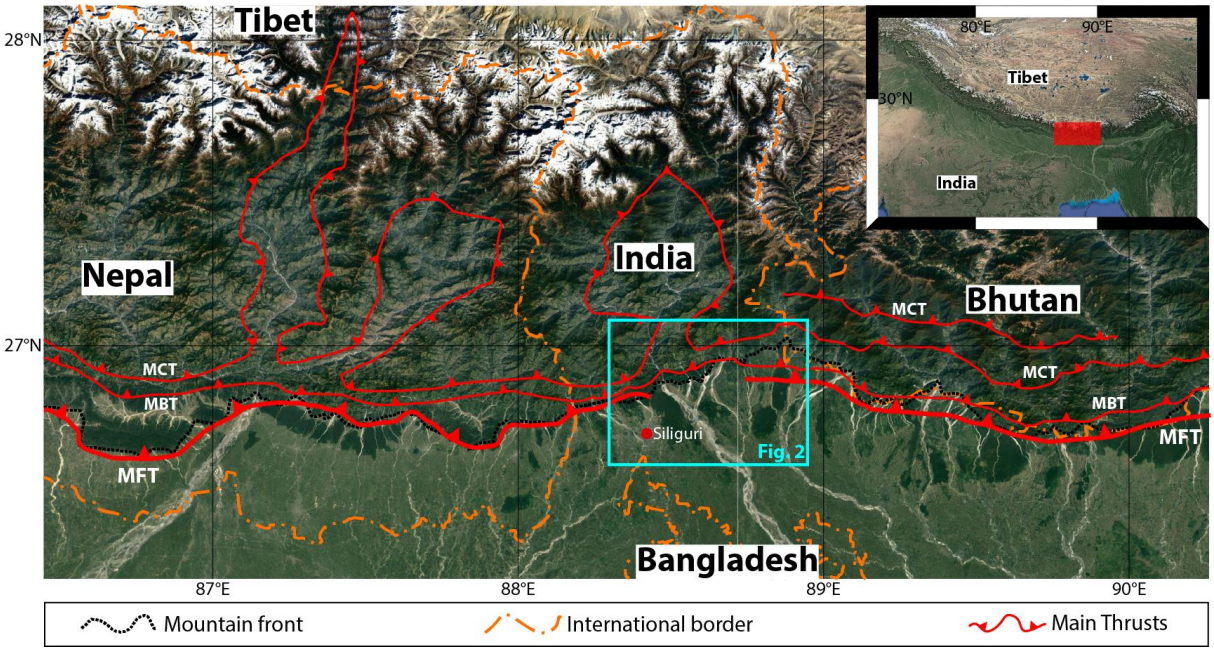

Figure 1: Overview of the study area. Top right inset shows by a red box the location of the map in the Himalayan range. Blue box shows location of Figure 2. Main thrusts of the Himalayan fault system shown in red: MCT for Main Central Thrust; MBT for Main Boundary thrust; MFT for Main Frontal Thrust. Locations of thrusts are from Tobgay et al. (2012) in Bhutan, Abrahami et al. (2018) in India and Mugnier et al. (2011) in Nepal.

2. Geomorphology and tectonics of the Darjeeling Himalayan piedmont

The southern emerging tip of the MHT places the Neogene synorogenic Siwalik Group, or less frequently the pre-orogenic rocks, over the modern quaternary alluvia of the Ganga-Brahmaputra plain along the Main Frontal Thrust (MFT) and the Main Boundary thrust (MBT) respectively, forming the southern important relief of the range, 300 to 400m above the plain. The Siwalik Group consists in an overall coarsening upward molassic sequence, its upper part being a moderately endured conglomeratic layer. The modern alluvia form fans and megafans at the outlet of the range which consist in poorly sorted and loosy sands to boulders beds (Dhital, 2015).

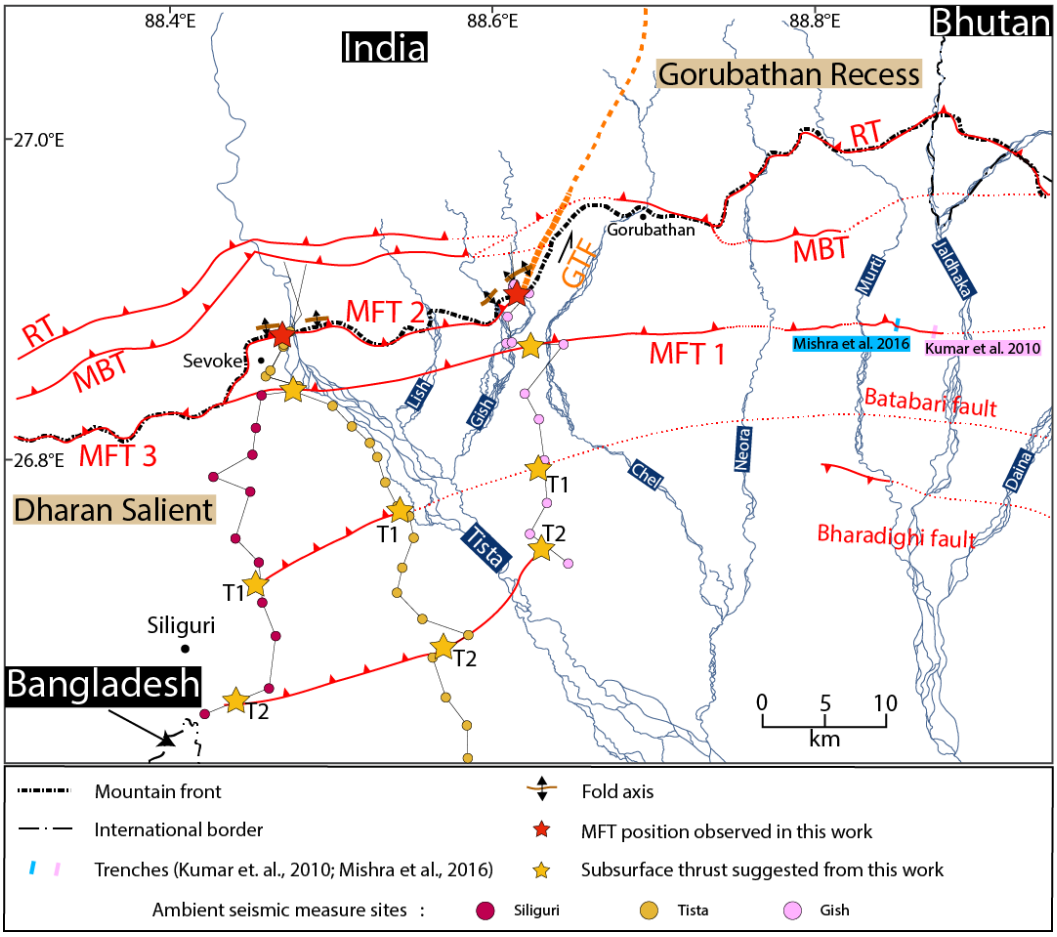

Figure 2: Structural map of the Darjeeling Himalayan Piedmont with location of the seismic profiles (see section 4 for their acquisition). The Gish Transverse Fault (GTF) separates the western Dharan salient from the eastern Gorubathan recess and is indicated by the orange line. Thrusts are represented in red. East of the GTF, the MBT, MFT1 and Bharadighi fault are from Nakata (1989). RT (Ramgarh Thrust) and Batabari fault are from Srivastava et al. (2017). West of the GTF, MFT1, T1 and T2 are suggested from HVSR geophysical data (see Figure 4B). MFT2 and MFT3 are respectively from personal field work, and Jayangondaperumal (personal communication), MBT and RT are from Mukul (2010).

Red, yellow and pink circles represent ambient noise seismic recording sites along the Siliguri, Tista and Gish profiles (respectively 17, 23 and 13 recording sites). See "Fig4_supporting information.kmz" for precise location of the profiles with the google earth software.

Our study is located in the Siliguri area, south of the Darjeeling Himalaya (Figure 1). There, the Himalayan mountain front is sinuous and characterized by the major Dharan salient and Gorubathan recess separated by the main Gish Transverse Fault (GTF) (Figure 2). The Quaternary alluvia are in contact with sedimentary rocks of the Siwalik group in the Dharan salient or with pre-orogenic rocks in the Gorubathan recess. East of the GTF, several active faults were described (Srivastava et al., 2017 and references therein): the MBT, MFT, the Batabari fault and the Bharadighi back-thrust (Figure 2). West of the GTF, the location of the active faults is still under discussion (Jayangondaperumal, personal communication). The late Quaternary alluvium of the Tista River onlaps the Siwaliks and seals the MFT (Abrahami et al., 2018), suggesting that the MFT has not been active since several kyrs. In contrast, geomorphologic markers suggest that the MBT fault system is still active (Mukul, 2000) in the Dharan salient. The Tista megafan ahead of the Himalayan front is strongly incised –about 37m– and the climatic or tectonically driven origin of this incision is still debated (Abrahami et al., 2018). Due to the strong vegetal cover of the area, geomorphologic studies are difficult although preliminary RTKGNSS (Real-Time Kinematic Global Network Satellite System) profiles (Figure 4A) suggest that scarps affect the top of the Tista megafan dated at 3.7 ± 0.7 ka (Abrahami et al., 2018). The HVSR method is therefore used to image the geometry of the structures beneath the Tista megafan and determine the origin of its incision.

3. Horizontal-to-Vertical Spectral ratio analysis of passive seismic records

Methods using seismic noise have been broadly used in the past decades for soil- structure interaction investigation (Guéguen et al., 2007; Hinzen et al., 2004; Paudyal et al., 2012), risk assessment (Bhandary et al., 2014), landslide characterization (Méric et al., 2007), building assessment (e.g., Guillier et al., 2014) and even for the exploration of Mars (Knapmeyer-Endrun et al., 2017). The HVSR method consists of using the seismic ambient noise

vibrations (Stehly et al., 2006) recorded at a single station, from which the ratio between the Fourier amplitude spectra of the horizontal (averaging NS and EW components) to vertical components are estimated.

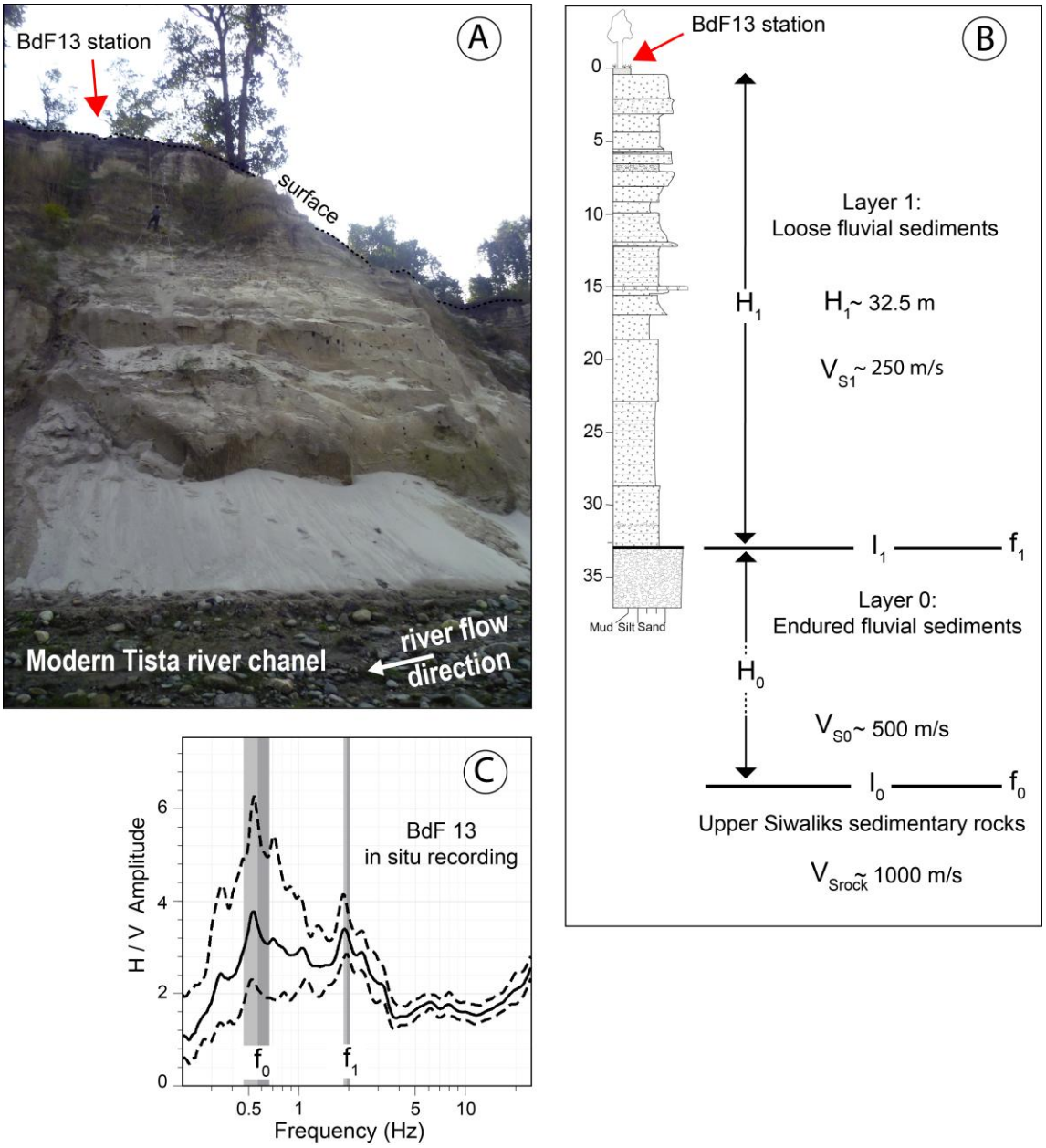

Figure 3: An example of foreland outcrops and of Horizontal-to-Vertical Spectral Ratio (HVSR) acquisition. (A) Picture of the incised sediment deposits of the Tista River (Darjeeling, Siliguri area). The red arrow refers to the location of the ambient vibration recording station (See Figure 3C). (B) Sedimentary log of the megafan incised by the Tista River. (C) Graph of the H/V spectral ratio amplitude versus frequency. The lowest frequency peak (f_0) is linked to the interface (I_0) between endured fluvial sediments and Upper Siwaliks

sedimentary rocks whereas the highest frequency peak (f_1) is linked to the interface (I_1) between loose fluvial sediments and endured fluvial sediments. Width of the light and dark gray bars on f_o and f_1 indicate the standard deviation. From the measured height H_1 of the cliff and the recorded frequency f_1, we calculated the velocity V_{S1}.

Seismic noise recordings were collected using a Cityshark II station connected to a 5 s. Lennartz seismometer, performing frequency analysis down to 0.2 Hz (Guillier et al., 2008). The sample frequency was set to 200 Hz with a duration of acquisition between 15 and 30 minutes (description of the data in Appendix A: supplementary data). The geopsy open-source pack software was used (www.geopsy.org; Wathelet et al., 2020). Recordings were processed using 50 s time windows, with a 5 % Tukey taper applied to both ends of each window and the individual HVSR curves were smoothed using the Konno and Ohmachi (1998) method with a constant of 40 before the computing of the final HVSR curve. As the frontal basin is very extended, we use a 1D model for the interpretation of the HVSR.

From each in situ recording, we obtain a HVSR curve (Figure 3C) from which one or two peaks are extracted: the fundamental frequency of the site (f_0) which is at the lowest frequency (following the recommendations in Bard, 2008) corresponding to the deeper interface and, when existing, a higher frequency (f_1) corresponding to a shallower interface. The determination of the main frequencies (f_0 and f_1) on the HVSR curve is automatically done by the *geopsy* software. The amplitudes of the peaks are directly linked to the difference of Shear-wave velocity (impedance contrast) at a lithological interface. From Bard's guidelines (2008), a peak can be identified on a HVSR curve only if its amplitude is higher than 2.0, meaning that the impedance contrast between the two layers permits the peak development (Albarello and Lunedei, 2013). Lower peaks are generally discarded unless there is a spatial continuity in the data.

161 If the HVSR curve displays only one peak, f_0 corresponds to the interface between a
162 superficial layer and a stiffer layer whatever its thickness.
163 The depth of the interface (H) is: $H = Vs / (4*f_x)$ (1)
164 where (f_x) is the peak frequency and (Vs) the Shear-wave velocity (Hinzen et al., 2004).
165 If two peaks are identified on the HVSR curve (Figure 3), the f_1 peak is interpreted as the
166 interface between a superficial loose layer, the thickness of which is directly calculated from
167 eq (1), and a stiffer sediment layer. The f_0 peak characterizes the interface between the latter
168 sediment layer and a third stiffer rock layer. The thickness of this layer is estimated from the
169 HVSR curve best fitting SH transfer function (SH being the Shear-wave polarized in the
170 horizontal plane) that is obtained from modeling with different thicknesses.
171
172 Table 1: Parameters used for SH transfer function computing.
173

LAYER	**Thickness (m)**	**Vp (m/s)**	**Vs (m/s)**	**Density (kg/m3)**	**Qp** Quality	**Qs** Factor
1 (loose sediments)	Defined by Eq.1	500	250	1800	50	25
0 (endured sediments)	Value to define	1000	500	2100	100	50
Rock (Siwaliks)	infinite	2000	1000	2500	200	100

174
175
176 The surface S-wave velocities are uncommonly obtained from drilling and assumptions
177 usually have to be made that depend on the lithology of the sediments, their compaction and
178 the burial depth. In this study, we performed an ambient seismic noise recording on a cliff
179 where the superficial boundary (the interface I_1 between loose sands and a conglomeratic
180 endured layer; Figure 3) was outcropping, therefore providing the height H_1 of the upmost
181 sand layer. From the depth H_1 of ~ 32.5 m and the frequency f_1 of ~ 1.9 Hz recorded from this
182 layer (Figure 3C), we calculated a corresponding Vs_1 of 250 m/s (eq. 1). As peak interfaces (I_1

and I_0) are well expressed, the corresponding impedance contrast at each interface should be ≥ 2.0 therefore providing a S-wave velocity Vs_0 ≈ 500m/s for the underlying endured fluvial sediment layer and a S-wave velocity Vs_{rock} ≈ 1000m/s in the Siwalik rocks.

Whatever the methodology to retrieve S-wave profile from HVSR spectrum (Arai and Tokimatsu, 2004; Bonnefoy-Claudet 2004; D'Amico et al., 2004; Picozzi et al., 2005; Gosar, 2017; van Ginkel et al., 2020), the thickness of the layer depends on the HVSR curves. When a single peak is displayed, the S-wave velocity down to the Siwalik rocks is of 500 m/s, allowing to derive directly the thickness of the upper layer from f_0 (Eq. 1). When a double peak is observed (Figure 3C), we derive H_1 ($\pm\boldsymbol{\sigma}$) from f_1 using Eq. (1) and Vs_1=250 m/s. Following Nakamura's (2019) interpretation, the HVSR curve is the transfer function of the soil. To define the thickness of the deeper endured fluvial sediment layer H_0, we proceeded by SH transfer function modeling (Wathelet et al., 2020; tool gpsh) which computing follows the reflectivity method (Kennet and Kerry, 1979) as implemented by Theodulidis et al. (1996). For such computing, it is needed for all layers: the thickness, Vp, Vs, Qp, Qs, and the density where Vs is known. Qs is estimated to Vs/10 (rule of thumb, Dal Moro, 2014; 2015) and Qp is estimated to 2Qs when the Vp/Vs is estimated to 2 (Gercek, 2017) and the density for layers 1, 0 and bedrock are respectively fixed to 1800, 2100 and 2500 kg/m^3 (Table 1). Finally, we compute the SH transfer function with different thicknesses, conserving the models with a lower frequency peak fitting in the f_0 ($\pm\boldsymbol{\sigma}$). This leads to an averaged thickness ($H_0\pm\boldsymbol{\sigma}$).

From the ambient seismic data acquired along the Tista and Gish rivers and their processing, we calculated the depth of the peak interfaces on a large area south of the mountain front and extracted the geometry of the underlying structures.

4. Subsurface structures inferred from HVSR method

208 The passive seismic data were acquired along three approximately N-S trending profiles
209 (Figure 2) located on the Tista megafan and the Gish Fan.
210 The results of the HVSR method show peaks of the H/V ratio at two different frequencies in
211 about 80% of the locations (Figure 4B), therefore indicating two interfaces with contrasted S-
212 wave velocities and three distinct layers. Following the method section, interface (I_1) was
213 attributed to a superficial contact within the Quaternary deposits (velocity contrast Vs_1/Vs_0)
214 and interface (I_0) to the contact between Quaternary sediments and the Neogene Siwalik
215 sedimentary rocks (velocity contrast Vs_0/Vs_{rock}) (Figures 3 and 4). The (I_1) shallowest
216 interface presents depths of a few meters to a few tens of meters. The (I_0) deeper interface
217 displays depths varying from ~100 to 600 m below the surface and globally deepens
218 southwards. Very close to the mountain front, it shows a complex pattern and its depth locally
219 changes abruptly (Figure 4B).
220

221 **5. Discussion: Interpretation of the HVSR data and comparison with the Tista megafan**
222 **morphology**

223 The interpretation of the HVSR data (Figure 4B infers that the top of the Siwaliks is affected
224 by thrusts and folds, a structuring already imaged by seismic reflections beneath the piedmont
225 of East-Central Himalaya (e.g., Duvall et al., 2020), where the thrust faults branch off the
226 same basal decollement as the MFT. The interpretation assumes that MFT and other thrust
227 faults dip ~20° northward (Almeida et al., 2018) and that the folds associated to the blind
228 thrusts have asymmetrical limbs, by analogy with the fault-related folds observed in the
229 Siwaliks (e.g., Mugnier et al., 1999). Three major thrusts are inferred along each profile
230 (Figure 4B) and their map pattern suggests that the northern thrust is located in the continuity
231 of scarps related to the MFT1 segment in the Gorubathan Recess (Nakata, 1989) and of the

MFT3 segments in the Dharan Salient (Figure 2). The T1 fault could be in the continuity of the Batabari fault.

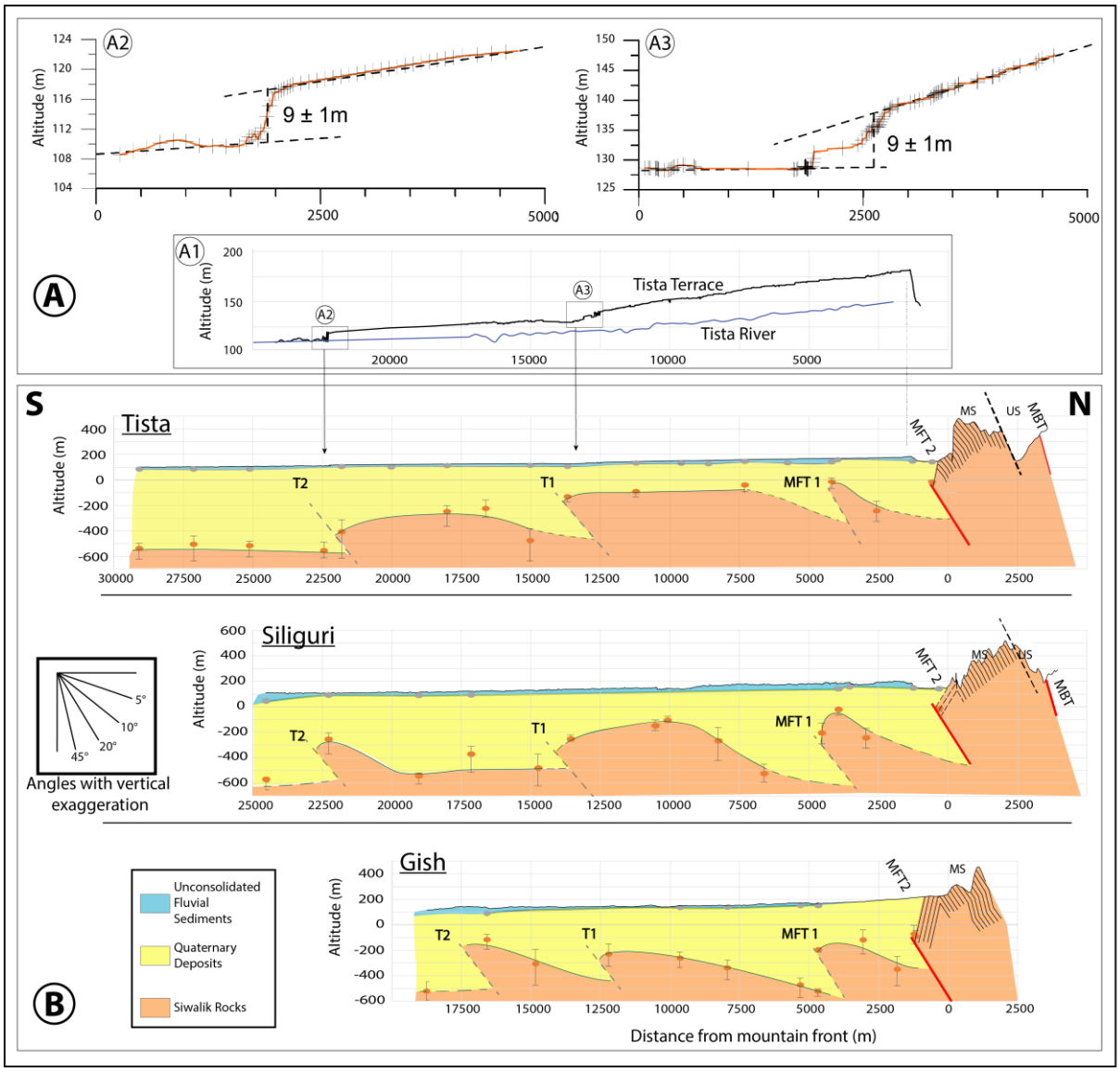

Figure 4: Morphologic profiles and subsurface structures inferred from HVSR method. (A1) Topographic profile through the Tista megafan drawn from our RTKGNSS data. Black rectangles A2 and A3 refer respectively to the topographic profile through the southern (A2) and northern (A3) scarps; in brown, profile from a weighted average of 20 RTKGNSS (Real-Time Kinematic Global Network Satellite System) data. (B) Ambient seismic data (See the data in "Fig.4B_Supporting Information.xls") from the Darjeeling area and their interpretation. Location of the data on figure 2. Dips of the Neogene Siwalik strata along the Gish and Tista sections are from our own data and Acharyya et al., (1987). Grey points correspond to the (I1) interface within Quaternary deposits; orange points and green lines

correspond to the (I0) interface which is interpreted as the Quaternary/Siwaliks contact. Suggested thrusts are represented in dashed gray lines. Note that the vertical scale is strongly exaggerated and the bottom left inset indicates the real values of the dips.

This interpretation suggests that two scarps, that are evidenced by geomorphologic profiles but nearly invisible in the jungle and that affect the Tista megafan with a total offset of ~ 18 ± 2m, would be related to the activity of the T1 and T2 thrusts (Figures 4A and 4B). Similar fault scarps, but more pronounced in height, were also evidenced eastward in the Gorubathan Recess piedmont and were associated to the surface ruptures of ~ A.D. 1100 (Kumar et al., 2010) and/or A.D. 1255 (Mishra et al., 2016) earthquakes (Figure 1). The two escarpments along the Tista profile could be linked to earthquakes occurring since the abandonment of the upper surface of the fan, dated at 3.7 ± 0.7 kyrs. Part of the Tista megafan incision is then linked to uplift along the faults related to these scarps and the rest of the 37 m could be due to climatic fluctuations (Abrahami et al., 2018) or to more distributed uplift. The mean uplift associated to each escarpment (Figure 4A) is at least 2.5 ± 0.8 mm/yr. Taking into account the structural studies of fault scarps (e.g., Jayangondaperumal et al., 2013), the slip beneath a scarp is at least twice the uplift, and the shortening absorbed by the two scarps would therefore be ~10 mm/yr, i.e., about half of the estimated Himalayan convergence (e.g., Lavé and Avouac, 2000).

6. Conclusions

We demonstrate that the HVSR method is a very powerful and simple tool that helps imaging the subsurface structures. In the case of the Darjeeling piedmont, our work allows a better mapping of the complex thrust network and shows that about half of the active shortening is distributed along several thrusts ahead of the Himalayan front. Nonetheless, the HVSR

method only records the major interfaces characterized by strong velocity contrasts and does not furnish a detailed picture of the structures. We therefore suggest that this method is only useful for preliminary mapping studies. It may indicate the key zones where more detailed surficial studies, such as GPR or trenching can be performed and allows to relate them with regional deeper structures, therefore improving the general knowledge of the Himalayan tectonics. Finally, it participates in identifying the active structures and is therefore of the upmost importance for assessing seismic hazard in densely populated regions.

Acknowledgments:

We acknowledge A. De Leeuw for numerous constructive discussions and an anonymous reviewer. We thank Dr. Sandip More for field assistance. This work has been funded by CNRS Himal-Fan ANR-17-CE01-0018 and in 2019 by an internal grant of the Institut des Sciences de la Terre (Grenoble). Maps were performed using the free Geographic Information System (www.qgis.org).

Declaration of Competing Interest:

The authors declare that there is no conflict of interest.

Data availability statement:

The data supporting the findings of this study are available on:

- Precise location of the passive seismic record sites in “Fig4_Supporting Information.kmz”
- Geophysical parameters and depths of the interface at each passive seismic record sites in “Fig4B_Supporting Information.xls”
- For the others data, they may be sent on request by the corresponding author.

References:

Abrahami, R., Huyghe, P., Van der Beek, P., Lowick, S., Carcaillet, J. and Chakraborty, T., 2018. Late Pleistocene – Holocene development of the Tista megafan (West Bengal, India): ^{10}Be cosmogenic and IRSL age constraints. *Quat. Sci. Rev.*, **185**, 69–90. doi: 10.1016/j.quascirev.2018.02.001

Acharyya, S.K., Bhatt, D.K. and Sen, M.K., 1987. Earliest Miocene planktonic foraminifera from Kalijhora area, Tista river section, Darjeeling Sub-Himalaya. *Indian Minerals*, **41**, 31–37.

Albarello, D. and Lunedei, E., 2013. Combining horizontal ambient vibration components for H/V spectral ratio estimates. *Geophys. J. Int.*, **194**, 936–951. doi: 10.1093/gji/ggt130

Almeida, R.V., Hubbard, J., Liberty, L., Foster, A. and Sapkota, S.N., 2018. Seismic imaging of the Main Frontal Thrust in Nepal reveals a shallow décollement and blind thrusting. *Earth Planet. Sci. Lett.*, **494**, 216–225. doi: 10.1016/j.epsl.2018.04.045

Arai, H. and Tokimatsu, K., 2004. S-wave velocity profiling by inversion of microtremor H/V spectrum. *Bull. Seismol. Soc. Am.*, **94**. doi: 10.1785/0120030028

Bard, P.-Y., 1999. Microtremor measurements: a tool for site effect estimation. *The effects of surface geology on seismic motion.*, **3**, 1251–1279.

Bard, P.-Y., 2008. Foreword: The H/V technique: capabilities and limitations based on the results of the SESAME project. *Bull. Earthq. Eng.*, **6**, 1–2. doi: 10.1007/s10518-008-9059-4

Bashyal, R.P., 1998. Petroleum exploration in Nepal. *J. of Nepal Geol. Soc.*, **18**, 19–24.

Bhandary, N.P., Yatabe, R., Yamamoto, K. and Paudyal, Y.R., 2014. Use of a Sparse Geo-Info Database and Ambient Ground Vibration Survey in earthquake disaster risk study: A case of Kathmandu Valley. *J. Civ. Eng. Res.*, **4**, 20–30. doi: 10.5923/c.jce.201402.03

Bilham, R., 2019. Himalayan earthquakes: a review of historical seismicity and early 21st century slip potential., *Geol. Soc. Lon. Spec. Publ.*, **483**, 423–482. doi: 10.1144/SP483.16

Bollinger, L., Sapkota, S.N., Tapponnier, P., Klinger, Y., Rizza, M., Van der Woerd, J., Tiwari, D.R., Pandey, R., Bitri, A. and Bes de Berc, S., 2014. Estimating the return times of great Himalayan earthquakes in eastern Nepal: Evidence from the Patu and Bardibas strands of the Main Frontal Thrust: Return period of Himalayan earthquakes. *J. Geophys. Res. Solid Earth*, **119**, 7123–7163. doi: 10.1002/2014JB010970

Bonnefoy-Claudet, S., 2004. Nature du bruit de fond sismique : implications pour les études des effets de site. Doctoral dissertation, Université Joseph Fourier , Grenoble, 241pp.

D'Amico, V., Picozzi, M., Albarello, D., Naso, G. and Tropenscovino, S., 2004. Quick estimates of soft sediment thicknesses from ambient noise horizontal to vertical spectral ratios: a case study in southern Italy. *J. Earthquake Eng.*, **08,** 895-908.

Dal Moro, G., 2014. Surface Wave Analysis for Near Surface Applications. Elsevier, Amsterdam. 250 pp. eBook ISBN: 9780128007709.

Dal Moro, G., 2015. Joint analysis of Rayleigh-wave dispersion and HVSR of lunar seismic data from the Apollo 14 and 16 sites. *Icarus*, **254**, 338–349. doi: 10.1016/j.icarus.2015.03.017

Dhital, M.R., 2015. Geology of the Nepal Himalaya - Regional Perspective of the Classic Collided Orogen. In: *Regional Geology Reviews* (Oberhänsli, R., de Wit, M.J. and Roure, F.M., eds) Springer International Publishing Switzerland. 498 pp. doi: 10.1007/978-3-319-02496-7

Duvall, M.J., Waldron, J.W.F., Godin, L., and Najman, Y., 2020. Active strike-slip faults and an outer frontal thrust in the Himalayan foreland basin, *PNAS*, **117**, 17615-17621. doi:10.1073/pnas.2001979117

Guéguen, P., Cornou, C., Garambois, S. and Banton, J., 2007. On the Limitation of the H/V Spectral Ratio Using Seismic Noise as an Exploration Tool: Application to the Grenoble Valley (France), a Small Apex Ratio Basin. *Pure Appl. Geophys.*, **164**, 115–134. doi: 10.1007/s00024-006-0151-x

306 Gercek, H., 2007. Poisson's ratio values for rocks. *Int. J. Rock Mech. Min. Sci.*, **44**. doi:
307 10.1016/j.ijrmms.2006.04.011

308 Gosar, A., 2017. Study on the applicability of the microtremor HVSR method to support
309 seismic microzonation in the town of Idrija (W Slovenia). *Nat. Hazards Earth Syst.*
310 *Sci.*, **17**. doi: 10.5194/nhess-17-925-2017

Guillier, B., Atakan, K., Chatelain, J.-L., Havskov, J., Ohrnberger, M., Cara, F., Duval, A.-M., Zacharopoulos, S., Teves-Costa, P. and the SESAME Team, 2008. Influence of instruments on the H/V spectral ratios of ambient vibrations. *Bull. Earthquake Eng.*, **6**, 3–31. doi: 10.1007/s10518-007-9039-0

Guillier, B., Chatelain, J.-L., Tavera, H., Perfettini, H., Ochoa, A. and Herrera, B., 2014. Establishing Empirical Period Formula for RC Buildings in Lima, Peru: Evidence for the Impact of Both the 1974 Lima Earthquake and the Application of the Peruvian Seismic Code on High-Rise Buildings. *Seismol. Res. Lett.***, 85**, 1308–1315. doi: 10.1785/0220140078

Hinzen, K.-G., Weber, B. and Scherbaum, F., 2004. On the resolution of H/V measurements to determine sediment thickness, a case study across a normal fault in the Lower Rhine

Embayment, Germany. *J. Earth. Eng.*, **08**, 909–926. doi: 10.1142/S136324690400178X

Jayangondaperumal, R., Mugnier, J.-L. and Dubey, A. K., 2013. Earthquake slip estimation from the scarp geometry of Himalayan Frontal Thrust, western Himalaya: Implications for seismic hazard assessment. *Int. J. Earth Sci.*, **102**, 1937–1955. doi: 10.1007/s00531-013-0888-2

Kennett, B. L. and Kerry, N. J., 1979. Seismic waves in stratified half space. *Geophys. J. R. Astron. Soc.*, **57**, 557-583. doi: 10.1111/j.1365-246X.1979.tb06779.x

Knapmeyer-Endrun, B., Golombek, M.P. and Ohrnberger, M., 2017. Rayleigh Wave Ellipticity Modeling and Inversion for Shallow Structure at the Proposed InSight Landing Site in Elysium Planitia, Mars. *Space Sci. Rev.*, **211**, 339–382. doi: 10.1007/s11214-016-0300-1

Konno, K. and Ohmachi, T., 1998. Ground-motion characteristics estimated from spectral ratio between horizontal and vertical components of microtremor. *Bull. Seismol. Soc. Am.*, **88**, 228–241.

Kumar, S., Wesnousky, S.G., Jayangondaperumal, R., Nakata, T., Kumahara, Y. and Singh, V., 2010. Paleoseismological evidence of surface faulting along the northeastern Himalayan front, India: Timing, size, and spatial extent of great earthquakes. *J. Geophys. Res.*, **115**, B12422. doi: 10.1029/2009JB006789

Lavé, J. and Avouac, J.P., 2000. Active folding of fluvial terraces across the Siwaliks Hills, Himalayas of central Nepal. *J. Geophys. Res.*, **105**, 5735–5770. doi: 10.1029/1999JB900292

Méric, O., Garambois, S., Malet, J.-P., Cadet, H., Guéguen, P. and Jongmans, D., 2007. Seismic noise-based methods for soft-rock landslide characterization. *Bull. Soc. Géol. Fr.*, **178**, 137–148. doi: 10.2113/gssgfbull.178.2.137

317 Mishra, R.L., Singh, I., Pandey, A., Rao, P.S., Sahoo, H.K. and Jayangondaperumal, R., 2016.
318 Paleoseismic evidence of a giant medieval earthquake in the eastern Himalaya:
319 Rupture Length of A.D. 1255 Earthquake. *Geophys. Res. Lett.*, **43**, 5707–5715. doi:
320 10.1002/2016GL068739

Mukul, M., 2000. The geometry and kinematics of the Main Boundary Thrust and related neotectonics in the Darjiling Himalayan fold-and-thrust belt, West Bengal, India. *J. Struct. Geol.*, **22**, 1261–1283. doi: 10.1016/S0191-8141(00)00032-8

Mukul, M., 2010. First-order kinematics of wedge-scale active Himalayan deformation: Insights from Darjiling–Sikkim–Tibet (DaSiT) wedge. *J. Asian Earth Sci.***, 39**, 645–657. doi: 10.1016/j.jseaes.2010.04.029

Mugnier, J.-L., Huyghe, P., Gajurel, A.P., Upreti, B.N. and Jouanne, F., 2011. Seismites in the Kathmandu basin and seismic hazard in central Himalaya. *Tectonophysics*, **509**, 33–49. https://doi.org/10.1016/j.tecto.2011.05.012

Mugnier, J.-L., Leturmy, P., Mascle, G., Huyghe, P., Chalaron, E., Vidal, G., Husson, L. and Delcaillau, B., 1999. The Siwaliks of western Nepal. *J. Asian Earth Sci.***, 17**, 629–642. doi: 10.1016/S1367-9120(99)00038-3

Nakamura, Y., 1989. A method for dynamic characteristics estimation of subsurface using microtremor on the ground surface. Quaterly Report Railway Techn. Res. Inst., **30**, 25-30.

321 Nakamura, Y., 2019. What is the Nakamura method? *Seismol. Res. Lett.*, **90**: 1437–1443. doi:
322 10.1785/0220180376

Nakata, T., 1989. Active faults of the Himalaya of India and Nepal. *Geol. Soc. Am.*, **232**, 243–264. doi: 10.1130/SPE232-p243

Pati, P., Parkash, B., Awasthi, A.K. and Jakhmola, R.P., 2012. Spatial and temporal distribution of inland fans/terminal fans between the Ghaghara and Kosi rivers indicate eastward shift of neotectonic activities along the Himalayan front. A study from parts of the upper and middle Gangetic plains, *India. Earth Sci. Rev.*, **115**, 201–216. doi: 10.1016/j.earscirev.2012.10.006

Paudyal, Y.R., Yatabe, R., Bhandary, N.P. and Dahal, R.K., 2012. A study of local amplification effect of soil layers on ground motion in the Kathmandu Valley using microtremor analysis. *Earthq. Eng. Eng. Vib.*, **11**, 257–268. doi: 10.1007/s11803-012-0115-3

Picozzi, M., Parolai, S. and Richwalski, S. M., 2005. Joint inversion of H/V ratios and dispersion curves from seismic noise: Estimating the S-wave velocity of bedrock. *Geophysical Res. Lett.*, **32**, L11308. doi: 10.1029/2005GL022878

Srivastava, V., Mukul, M. and Mukul, M., 2017. Quaternary deformation in the Gorubathan recess: Insights on the structural and landscape evolution in the frontal Darjiling Himalaya. *Quat. Int.*, **462**, 138–161. doi: 10.1016/j.quaint.2017.05.004

Stehly, L., Campillo, M. and Shapiro, N.M., 2006. A study of the seismic noise from its long-range correlation properties. *J. Geophys. Res.*, **111**, B10306. doi: 10.1029/2005JB004237

Theodulidis, N., Bard, P.-Y., Archuleta, R.J. and Bouchon, M., 1996. Horizontal to vertical spectral ratio and geological conditions: the case of Garner Valley downhole array in Southern California. Bull. *Seism. Soc. Am.*, **86**, 306-319. doi: 10.1785/BSSA0860020306

Tobgay, T., McQuarrie, N., Long, S., Kohn, M.J. and Corrie, S.L., 2012. The age and rate of displacement along the Main Central Thrust in the western Bhutan Himalaya. *Earth Planet. Sci. Lett.*, **319–320**, 146–158. https://doi.org/10.1016/j.epsl.2011.12.005

van Ginkel, J., Ruigrok ,E. and Herber, R., 2020. Using Horizontal to Vertical Spectral Ratios to construct shear-wave velocity profiles. *Solid Earth*, **11**, 2015-2030. doi: 10.5194/se-11-2015-2020

Wathelet, M., Chatelain, J.-L., Cornou, C., Giulio, G.D., Guillier, B., Ohrnberger, M.ans Savvaidis, A., 2020. Geopsy: A User-Friendly Open-Source Tool Set for Ambient Vibration Processing. *Seismol. Res. Lett.***, 91**, 1878–1889. doi: 10.1785/0220190360

Figure 3: An example of foreland outcrops and of Horizontal-to-Vertical Spectral Ratio (HVSR) acquisition. (A) Picture of the incised sediment deposits of the Tista River (Darjeeling, Siliguri area). The red arrow refers to the location of the ambient vibration recording station (See Figure 3C). (B) Sedimentary log of the megafan incised by the Tista River. (C) Graph of the H/V spectral ratio amplitude versus frequency. The lowest frequency peak (f_0) is linked to the interface (I_0) between endured fluvial sediments and Upper Siwaliks sedimentary rocks whereas the highest frequency peak (f_1) is linked to the interface (I_1) between loose fluvial sediments and endured fluvial sediments. Width of the light and dark gray bars on f_o and f_1 indicate the standard deviation. From the measured height H_1 of the cliff and the recorded frequency f_1, we calculated the velocity V_{S1}.